

The formation of periodic three-body orbits for Newtonian systems

Simon Portegies Zwart^{1*}, Arjen Doelman², and Jelmer Stein³,

¹ Leiden Observatory, Leiden University, PO Box 9513, 2300 RA, Leiden, The Netherlands

² Mathematisch instituut, Leiden University, PO Box 9513, 2300 RA, Leiden, The Netherlands

³ Niels Bohr International Academy, University of Copenhagen, Copenhagen, Denmark

January 16, 2026

ABSTRACT

Context. Braids are periodic solutions to the general N-body problem in gravitational dynamics. These solutions seem special and unique, but they may result from rather usual encounters between four bodies.

Aims. We aim at understanding the existence of braids in the Galaxy by reverse engineering the interactions in which they formed.

Methods. We carry out simulations of self-gravitating systems of N particles using 4-th order integration. These simulations start by constructing the specific braid, and subsequently bombard it with a single object. We subsequently study how frequently the bombarded braid dissolves in four singles, a triple and a single, a binary and two singles, or two binaries. The relative proportion of those events gives us insight into how easy it is to generate a braid through the reverse process.

Results. It turns out that braids are relatively easily generated from encounters between two binaries, or a triple with a single object so long as they meet each other, independent on the braid's stability. We find that three of the explored braids are long-lived and linearly stable against small perturbations, whereas one is unstable and short-lived. The shortest-lived braid appears the least stable and the most chaotic. Also nonplanar encounters can lead to braid formation, which, in our experiments, themselves are planar. The parameter space in azimuth and polar angle that lead to braid formation via binary-binary or triple-single encounters is anisotropic, and the distribution has a low fractal dimension.

Conclusions. Since a substantial fraction of $\sim 9\%$ of our calculations lead to periodic three-body systems, braids may be more common than expected. They could easily temporarily exist as a result of multi-body (binary-binary or triple-single) interactions. We do not expect many stable braids to exist for an extensive period of time, but they may be quite common as transients, as they survive for tens to hundreds of periodic orbits. We argue that braids are particularly common in relatively shallow-potential background fields, such as the Oort cloud or the Galactic halo. Braid formation, however, easily leads to collisions between two or more of its constituents. If composed of compact objects, they potentially form interesting targets for gravitational wave detectors.

Key words. braids; multi-body interactions; gravitational dynamics; transients

1. Introduction

The gravitational N-body problem originated when Newton presented his theory of gravity (Newton 1687). Newton was able to analytically calculate periodic solutions of the two-body problem. We call these Kepler orbits (Kepler 1609); two objects in a periodic bound orbit in an elliptical trajectory around their common center of mass. For $N > 2$, such periodic solutions exist, but they are hard to find.

Negative total energy alone is insufficient as a criterion to determine the long-term stability of a ≥ 3 body problem because the system is chaotic and therefore evolves in finite time to the ejection of one object, leaving the other two bound in a pair Poincaré (1891). Euler and Lagrange, however, found potentially long-lived periodic solutions to the three-body problem (see also Henon 1976). These choreographies were later identified as belonging to the same family of periodic solutions (Montgomery 1998). Although so far, only periodic solutions turned out to be possibly long-term stable, there is no theorem to prove this (Terracini 2022).

More than a century later Moore (1993) proposes a topological classification as a tool for extending the “symbolic dynamics” approach to many-body dynamics. He described the Figure-8 (not to confuse with figure 8, which shows the initial azimuth and polar angle distribution for successful braid formation) solution of the gravitational N-body problem as a braid. Braids are periodic, reducible, and pseudo-Anosov orbits of the gravitational N-body problem (Kajihara et al. 2023). Such a braid emerges once all bodies in the system are given the same velocity vector and present their orbits as strands in time and one spatial coordinate. The form of the Figure-8 then becomes $(b_1 b_2^{-1})^3$, where b_i corresponds to the crossing the i -th strand over the $(i+1)$ st (Moore 1993). The stability of such primitive braids was further studied by Simó (1994), who argues that some have relative equilibrium solutions. In astronomical terms, we would describe a braid as a non-hierarchical periodic solution of the N-body problem.

Simó (2001) makes the distinction between “linearly stable”, and “unstable” choreographies. Of the 18 tested, he found that only the Figure-8 is stable. This finding is consistent with that of Schubart (1956).

Chenciner et al. (2002) makes the distinction between a simple choreography, of the N-body problem, which in their defini-

* Neither of the authors could have done this work without the other two

tion is “*a periodic solution in which all N masses trace the same curve without colliding*”, and choreographies of arbitrary complexity or symmetry. Both choreographies exist (Chenciner et al. 2002), although their stability and frequency remain uncertain (Simó 2002). Kapela & Simó (2007) continued on this work by studying the stability of complex (non-symmetric) braids composed of 7 bodies. They found that such choreographies can be dynamically stable.

The astro-dynamical community became aware of the work on braids through the discussion by Chenciner & Montgomery (2000), who further addressed the Figure-8 periodic solution. They, however, did not provide proof for the Figure-8’s long-term stability. Such proof was provided in Kapela & Simó (2007), who demonstrated linear stability of the Figure-8 orbit.

In the years since, many new braids of various types were found. Nowadays, most braids are discovered using supercomputers. Li et al. (2018) found 1223 new solutions, which were later expanded with another 13315 by Li et al. (2021). We conjecture that there exist an infinite number of possible (distinct) periodic solutions to the general N -body problem. However, only a subset of those are expected to be stable against small perturbations, and we then still expect an infinite number of stable periodic orbits.

Although claimed to be stable by Li et al. (2021), it is not a priori clear to what degree these braids are long-term stable. The lack of stable braids does not necessarily mean that they do not exist in the Universe. But if they exist, it may be non-trivial to recognize them. We follow up on the work of Heggie (2000) who considered the possibility that the Figure-8 braid formed from two encountering pairs of objects. In this case, objects could be black holes, stars, planets, planetesimals, or any set of massive objects.

For our calculations, we adopt Newton’s equations of motion with point-masses and integrated using a 4th order numerical scheme. This poses some limitations to the interpretation of our results, as astronomical objects tend to have properties that cause them to interact non-Newtonianly, such as finite radii, their orbits are affected by general relativistic effect, and radiation pressure¹. The effect of numerical errors, and accuracy in relation to the chaotic dynamics is discussed in section 4.7.

2. Initial conditions and model parameters

2.1. Initial conditions

We adopt a similar approach as proposed in Heggie (2000), by integrating a three-body braid, and bombarding it with a fourth particle. Since Newton’s equations of motion are time symmetric, the inverse interaction then results in a braid, while the original bomb escapes. Heggie (2000) used this strategy to explain how the Figure-8 braid can form from two interacting binaries. We take a more general approach in which we cover a larger part of the initial parameter space. In the main part of our study, we reduce the initial parameter space by limiting ourselves to interactions in the $x - y$ plane, leaving the z coordinate and the velocity perpendicular to the plane is equal to zero. (Note that it is not known if non-planar braids exist.) We further fix the braid’s orbital phase and orientation, but allow the incoming object to come from any azimuthal direction θ . We randomize in this direction. We relax the assumption on planar encounters in section 4.5, where we discuss the anisotropy of the initial parameter space.

¹ We follow Orwell’s *Ignorance is strength* philosophy in this perspective (Orwell 1949, see p.6).

2.2. Parameterics

Once the braid (see figure 1) is specified, the mass m_4 , velocity v_4 , impact parameter d , and initial distance r of the incoming fourth object remain free to vary. For initial conditions we then have $v_4(t = 0) \equiv v_{\text{in}}$, $m_4(t = 0) \equiv m_{\text{in}}$, and $d_4(t = 0) \equiv d_{\text{in}}$. Note that if the velocity at infinity satisfies $v_{\text{in}} = 0$, the impact parameter d_{in} becomes meaningless. Here units are dimensionless, adopting N -body units following Hénon-Heggie, i.e., $G = 1$ (Heggie & Mathieu 1986).

Simulations are continued until one object (or the center of mass of a binary or triple) satisfies the following conditions: it is farther than 1000 N -body units from the center of mass of the four-body system and it is receding from the system with a velocity exceeding the escape speed.

It is worth noting that the braid can formally be unbound if an incoming object’s kinetic energy exceeds the braid’s binding energy. For the braids in our experiments, this is the case if the incoming object has mass $m_{\text{in}} = 1$ with velocity $v_{\text{in}} \gtrsim 1.7$. An incoming object with even higher velocity can unbind the braid into four single objects. Unbinding the braid, however, requires efficient energy transfer from the incoming object to the particles in the braid, which is not common (see table 2). Table 2 also lists the total number of calculations performed, and the fractions of the various resulting configurations.

2.3. Classifying braids

Apart from the Figure-8 braid, we consider two more complex braids, listed in Li et al. (2018) $I.A.4^{i.c.}(0.5)$, and $I.A.68^{i.c.}(0.5)$. These names stand for the class of braid, with in parentheses the mass of the third particle (m_3) assuming $m_1 = m_2 = 1$. The initial conditions for these braids can be written as follows: $\mathbf{r}_1 = (-1, 0) = -\mathbf{r}_2$. $\mathbf{v}_1 = (\xi_a, \xi_b) = -\mathbf{v}_2$. Here $\mathbf{r}_i \equiv (x_i, y_i)$ is the two-dimensional Cartesian position vector, and equivalently for \mathbf{v}_i . The two scalars ξ_a , and ξ_b , characterize the interaction. For the incoming third particle $\mathbf{r}_3 = (0, 0)$, and $\mathbf{v}_3 = (2\xi_1/m_3, -2\xi_2/m_3)$. All z coordinates and velocities v_z are zero (but see section 4.5).

We include a fourth braid with unequal masses, $m_1 = 0.87$, $m_2 = 0.80$, and $m_3 = 1$, which is presented in table 1 of Li et al. (2021). The initial conditions for the braids we explored are presented in table 1.

3. Numerical integration

We perform the numerical integration using the Astrophysics Multipurpose Software Environment (AMUSE) (Portegies Zwart et al. 2009; Portegies Zwart & McMillan 2018) with the direct 4th order Hermite predictor-corrector N -body solver Ph4 (McMillan et al. 2012; Portegies Zwart et al. 2022). The calculations are performed using point masses with a time-step parameter of $\eta = 0.01$, and zero softening. In figure 1 we illustrate the braids integrated for one orbit, and in section 4.7 we discuss the effect of numerical precision on the results.

In figure 2 we present $I.A.4^{i.c.}(0.5)$ after 100 N -body time units. By this time, the orbit cannot be classified as a braid; the orbit is not periodic. In the next few 100 time units, one of the three particles is ejected, leaving the other two orbiting their joined center of mass.

Figure 3 shows a distinctly different evolution for Model A (the unequal-mass braid case) after 10^6 time units. By this time, the orbit is still stable, and the orbital shape is indistinguishable

m	x	y	v_x	v_y
Figure-8 problem (top panel in figure 1)				
1	0.9700436	-0.24308753	0.466203685	0.43236573
1	-0.9700436	0.24308753	0.466203685	0.43236573
1	0	0	0.93240737	0.86473146
Non-equal-mass problem (= model A, second panel in figure 1)				
0.87	-0.1855174644	0	0	2.0221546880
0.80	1	0	0	0.3968976468
1.0	0	0	-2.25026390304	0
AI4(0.5) (third panel in figure 1)				
1	-1	0	0.2009656237	0.2431076328
1	1	0	0.2009656237	0.2431076328
0.5	0	0	-0.8038624948	-0.9724305312
AI68(0.5) (bottom panel in figure 1)				
1	-1	0	0.2138410831	0.0542938396
1	1	0	0.2138410831	0.0542938396
0.5	0	0	-0.8553643324	-0.2171753584

Table 1. Four braids used in this study. The figure 8, Model A (one of the non-equal-mass cases from Li et al. 2021), $I.A.4^{i.c.}(0.5)$, and $I.A.68^{i.c.}(0.5)$. Presented for these braids are the mass of the three components m , the Cartesian positions x , and y , and the corresponding velocities v_x , and v_y . For all particles the Cartesian coordinate $z = 0$, and velocity $v_z = 0$.

from the original orbit, except that it has been subject to precession. We integrated the orbit twice, once with a perturbation of 10^{-5} to one of the particle's x-coordinates. However, upon optical inspection, both orbits are still indistinguishable after integrating for $t = 10^6$.

4. Results

4.1. Braid stability

We determine the stability of a braid by integrating it twice; Once with the canonical initial realization (see table 1), and once with a small perturbation by translating one particle 10^{-5} along the x-axis. Both integrations are continued for 10^5 N-body time units, and we determine the Lyapunov time scale by fitting a straight line to the logarithm of the geometric distance evolution in time. The results are presented in table 2.

The phase-space distance of an initially introduced perturbation in $I.A.4^{i.c.}(0.5)$ grows exponentially, as one would expect for a chaotic system. The Lyapunov time scale for this braid is ~ 13 orbits. The other models, Figure-8, Model A, and braid $I.A.68^{i.c.}(0.5)$, are linearly stable against infinitesimal perturbations. Note that for braid $I.A.68^{i.c.}(0.5)$ $t_{\text{stable}} \gtrsim 9.10^4$ (see table 2), which strictly speaking doesn't make it linearly stable, but the accumulation errors in our numerical integration may here drive the system's instability. Such numerical errors can be mitigated by integrating the braid using arbitrary precision arithmetic, as is explored in Boekholt & Portegies Zwart (2015), which is beyond this paper's scope.

Interestingly enough, the growth for model A makes periodic excursions, to shrink to values comparable to the initially introduced perturbation (10^{-5}). The time scale of these excursions is about ~ 3850 time units, or 642 orbits. This curious behavior can be interpreted as the system being stable against small variations in orbital phase. Even after integrating the system for a million time units it still exhibits the same curious behavior. This corresponds roughly to a 5-minute variation in the Earth's orbit around the Sun. Such quasi-periodic periodic behavior of excursions in shrinking and stabilizing, with a well-defined time scale, is a hallmark signature of a Neimark-Sacker bifurcation –

the discrete time analogue of the Hopf bifurcation (Homburg & Knobloch 2024).

4.2. Braid formation

The majority of interactions result in a binary with two single objects, while the other three possibilities have comparable probability. (Note that interactions leading to four single stars, 4S interactions, only occur for sufficiently large incoming velocities.) The relative branching ratios of the encounter results are quite comparable for each of our selected braids, and this measure appears independent of the braid's stability. On average, 4 to 6 % of the braids fall apart to a binary-binary, consistent with the earlier results by Heggie (2000) for the Figure-8 problem. We also find a somewhat lower fraction of braids (of ~ 2 to ~ 4 %) that dissolve into a triple-single. Both these solutions are of interest for generating braids from the reverse interaction.

In figure 4, we present the three most common interactions that lead to braid-formation, which are a braid $I.A.4^{i.c.}(0.5)$ by bombarding a binary with two single stars, two binaries that encounter each other to make the Figure-8 (as in Heggie (2000)), or forming a braid $I.A.4^{i.c.}(0.5)$ by a single object injected into a triple.

4.3. Braid progenitors

In figure 5, we present the orbital separations of the two binaries for braid Model A, the one with a $f_{BB} = 0.83$ in table 2 or 242 binary pairs. The inner and outer binaries have $\langle a_{\text{in}} \rangle \simeq 0.30$ with a median of $a_{\text{in}} = 0.24^{+0.47}_{-0.14}$. For the outer orbit we find $\langle a_{\text{out}} = \rangle \simeq 52$ with a median of $a_{\text{out}} = 1.84^{+21.34}_{-0.46}$. For the other braids, the media have a similar range. It turns out that braids tend to dissolve in a very tight and one very wide binary. Equally wise, braids tend to dissolve in a hierarchical triple (one with a tight inner a rather wide outer orbit).

The eccentricity (e) distribution of the two binaries in which a braid separates is strongly peaked towards unity. Objects in our calculations were point masses, and collisions or gravitational wave radiation were ignored. But if we were to introduce (reasonable) finite radii, $\gtrsim 10\%$ of interactions would lead to col-

Model	E	t_{peri}	t_L	t_{stable}	N	f_{BSS}	f_{4S}	f_{BB}	f_{TS}	stability
Figure-8	-1.29	6.33	$\lesssim 3 \cdot 10^4$	$> 10^5$	4380	0.833	0.079	0.064	0.025	linear stable
Model A	-2.08	5.99	$\gtrsim 3 \cdot 10^4$	$> 10^5$	4175	0.817	0.078	0.083	0.022	linear stable
$I.A.4^{i.c.}(0.5)$	-1.00	19.01	$\lesssim 2 \cdot 10^2$	$\lesssim 40$	3624	0.877	0.055	0.037	0.031	unstable
$I.A.68^{i.c.}(0.5)$	-1.26	83.85	$\sim 10^4$	$\lesssim 9 \cdot 10^4$	3020	0.803	0.094	0.064	0.039	marginally stable

Table 2. Integration result for the various braids, integrated using the 4th order Hermite predictor corrector for 10^4 N-body time units with a time-step parameter of $\eta = 0.01$, and with outputs every 0.1 time unit. The first column identifies the interaction, followed by the braid's total energy in N-body units [mass·(length/time) 2], and the period of one complete orbit. The Lyapunov time scale (fourth column) was calculated by introducing a small perturbation (of 10^{-5}) in the x-coordinate of the first particle. The fifth column gives t_{stable} , the integration time over which we could determine that the system remained stable with a maximum integration time of $t_{\text{stable}} = 10^4$. Note that we classify $I.A.68^{i.c.}(0.5)$ as marginally stable, discussed in section 4.1. The following column gives the number of experiments calculated while varying m_{in} , the impact parameter and relative encounter velocity. The last 4 columns give the fraction of interaction that leads to the various outcomes (marginalized over v_{in} , m_{in} , and d_{in}), binary-single-single (BSS), four single stars (4S), binary-binary (BB), and triple-single (TS).

lisions, rather than a stable pair of binaries. To guide the eye, and illustrate the skewness of the eccentricity distribution, we overplot curves for $f(e) \propto e^2, \propto e^3$, and $\propto e^4$, in figure 5. A distribution $f(e) \propto e^2$ would naively be consistent with expectations based on virialized few-body scattering (Heggie 1975). However a steeper distribution towards high eccentricities is expected for encounters between hard pairs of particles (Ginat & Perets 2024). It raises the intriguing possibility that a braid could form from a 4-body encounter in which two objects experience a collision, leaving the collision product and the other unaffected objects in a braid.

4.4. Braid formation cross section

In figure 6 we present the interaction result from launching particle $m_4(t = 0) \equiv m_{\text{in}}$, with velocity v_{in} , and impact parameter d_{in} into the braid from Model A. We performed 6 series of calculations for each parameter, marginalizing over the direction ϕ from which the particle was injected. We performed similar calculations for the other braids, but the figures are insufficiently different to present. Except for the effect of v_{in} for braid $I.A.68^{i.c.}(0.5)$, which we present in figure 7, showing quite different results. It is interesting to note that, together with the Figure-8, this braid is linearly stable.

The circles with outcome statistics in figure 6 illustrates irregularity in the solution space. Although outcomes are dominated by binary and two single escapers (green circles), the binary-binary formation channel and triple-single channel are prevalent. For this model, when the incoming velocity $v_4 \gtrsim 4$, encounters fail to result in two binaries.

On the other hand, even higher incoming velocities tend to lead to the survival of the braid, rather than to the formation of a hierarchical triple. In figure 6 we do not make the distinction between a surviving braid (democratic triple) and the more usual outcome in the form of a hierarchical triple; both are indicated by a red dots in figure 6. This trend is even more pronounced in figure 7, where the braids in the outermost ring (highest incoming velocity) survives in 22.8% of the cases. When injected along the braid's long axis, the encounter tends to lead to a binary and two singles, or four singles. In figure 7 we present the simulation results for braid $I.A.68^{i.c.}(0.5)$ with v_4 as the free parameter. One of the striking differences compared to figure 6 is the relatively large proportion of triples formed when the velocity of the incoming particle, $|v_4| \gtrsim 8$.

However, when injected perpendicular to the braid's long axis (around $45^\circ \lesssim \phi \lesssim 135^\circ$ and $225^\circ \lesssim \phi \lesssim 315^\circ$) the encountering objects tend to fly through the braid without doing much damage. The other models (Figure-8, Model A, and

$I.A.4^{i.c.}(0.5)$) being more symmetric, are less prone to such harmless penetrating encounters. It is interesting to note that the survivability of the braid (or the preservation of the democratic triple) as a result of a penetrating encounter seems not to depend on stability, or the Lyapunov time scale.

4.5. The third dimension

So far we studied the planar problem, in which all participating particles are in the same plane. Since this is rather restricted, we also explore the possibility forming a planar braid given a non-planar interaction. We realize this by injecting the incoming particle from a random direction into the planar braid. In this experiment the braid is orbiting in the X-Y Cartesian plane with zero azimuth ($\theta = 0$). The incoming particle is injected isotropically from azimuth $\theta \in [-180^\circ, 180^\circ]$ and polar angle $\phi \in [-90^\circ, 90^\circ]$. In figure 8 we present the Mollweide projection of one such cases for the Figure-8 problem for two incoming velocities: $v_{\text{in}} = 0$, and $v_{\text{in}} = 2$.

The fraction of interactions that produce braids in the non-planar case is statistically indistinguishable from that in the planar case, for binary-binary as well as for the triple-single encounters.

Certain areas in parameter space are preferred for specific interactions. This trend becomes even more pronounced for higher initial incoming velocities. For the Figure-8 solutions (adopting $m_{\text{in}} = 1$, and $d_{\text{in}} = 0$) braids, a low value of $v_{\text{in}} = 0$ does not lead to an appreciable anisotropy in the initial conditions for forming braids either from binary-binary or triple-single encounters. However, as illustrated in figure 8, for $v_{\text{in}} = 2$ binary-binary encounters are significantly more concentrated to low values of the azimuth and polar angles. This trend of clustering is comparably pronounced in the model-A, and $I.A.68^{i.c.}(0.5)$ braids, but is notoriously absent for $I.A.4^{i.c.}(0.5)$, which does not show this

To test the anisotropic distribution of the various simulation results, we check if the mean vector length is close to zero using the Rayleigh test for uniformity on the sphere. Under isotropy, the test statistic R^2/N (where R is the resultant vector length and N is the number of points) should be $\lesssim 3$ (for sufficiently large N). The results of this analysis are presented in table 3.

4.6. The fractality of the initial phase-space

The distribution of the incoming angles suggest a fractal distribution in parameter space. For that reason we calculate the fractal (box counting) dimension (D) for each of the distributions in table 3. To quantify this statement, we present in figure 8 the fractal dimension by mapping the azimuth and polar angles on

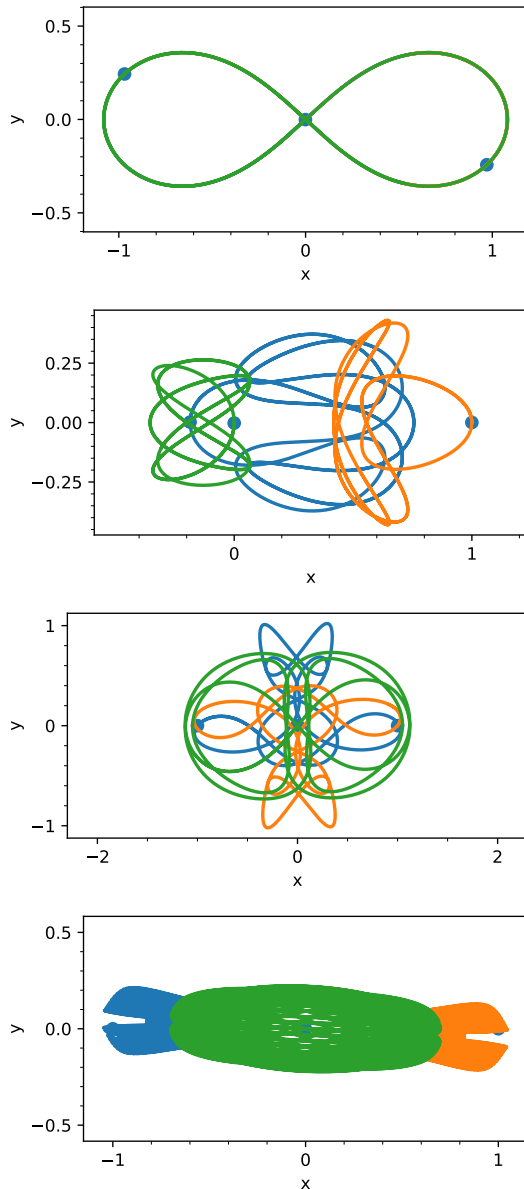


Fig. 1. The four 3-body braids adopted in this study. The classic Figure-8 (top panel) problem, and the three more complicated braids, the unequal-mass problem, $I.A.4^{i.c.}(0.5)$, and $I.A.68^{i.c.}(0.5)$ for the bottom panel. Integrated with a time-step parameter of $\eta = 0.01$, a time step of $dt = 0.001$, and integrated for one periodic orbit. The bottom panel shows $I.A.68^{i.c.}(0.5)$, which is a complex orbit for which the period exceeds 83 time units, much more than any of the others. The orbit closes only after many orbits, giving rise to the filled-in surfaces. For the Figure-8, only one line color is visible, because all three objects have the same orbit and therefore overlap.

a two dimensional grid, and subsequently apply box-counting to estimate the fractal dimension from how the number of occupied boxes scales with box size. The results are presented in table 4.

All binary-single-single encounters correspond to a fractal dimension $D \sim 1$: the resulting parameter space maps homogeneously on azimuth and polar angle. We saw this already in relation to figure 8 (green circles), and the Rayleigh test results in table 3. The binary-binary and triple-single encounters, however, (irrespective of braid model or the incoming velocity v_{in}) are clustered or lie along a curve in azimuth and polar angles, rather than a uniform filling of the parameter space. Although

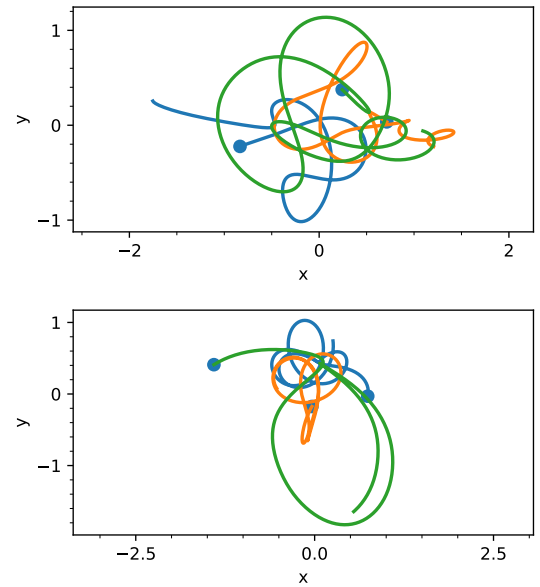


Fig. 2. Two representations of braid $I.A.4^{i.c.}(0.5)$ after 100 time units. The top panel shows the unperturbed solution integrated for 10 N-body time units. The bottom panel shows the result of the perturbed solution in the same time frame. The introduced perturbation was 10^{-5} in the x -coordinate. Both solutions have clearly deviated from the original braid, and from each other. By this time, the phase space distance between the two solutions is on the order of unity. The orbits are unstable, and in the next 100 crossing time, one particle is ejected.

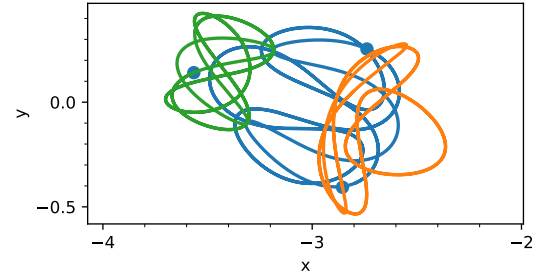


Fig. 3. Braid model A after 10^6 N-body time units. By this time, an initial perturbation of 10^{-5} has grown to $O(10^{-2})$. The braid still resembles the original, but the entire orbit has been precessing.

Model	$v_{in} = 0$			$v_{in} = 2$		
	R_{BSS}	R_{BB}	R_{TS}	R_{BSS}	R_{BB}	R_{TS}
Figure-8	0.4	2.7	0.6	4.3	15.7	4.9
Model A	1.5	1.6	0.8	5.8	12.1	1.2
$I.A.4^{i.c.}(0.5)$	1.6	0.3	3.4	0.1	0.6	0.8
$I.A.68^{i.c.}(0.5)$	2.1	1.8	3.1	1.1	6.1	2.5

Table 3. Chi-squared values for Rayleigh test (3 degrees of freedom) for spherical isotropy in azimuth and polar angles for the various simulation outcomes for braids Figure-8, Model A, $I.A.4^{i.c.}(0.5)$, and $I.A.68^{i.c.}(0.5)$. We performed 300 simulations for each set of initial conditions. Both sets adopted $m_{in} = 1$, and $d_{in} = 0$. The left set of runs was performed using the incoming velocity $v_{in} = 0$, the right set using $v_{in} = 2$. Here R_{BSS} , R_{BB} , and R_{TS} give the value of Rayleigh Chi-squared for the binary-single-single, binary-binary, and triple-single results. Note, the null hypothesis (consistent with isotropy) is met for values $\ll 3$. For values $\gg 3$ the distribution is evidently anisotropic. Note that in all cases $p < 0.05$, indicating that our results are statistically significant.

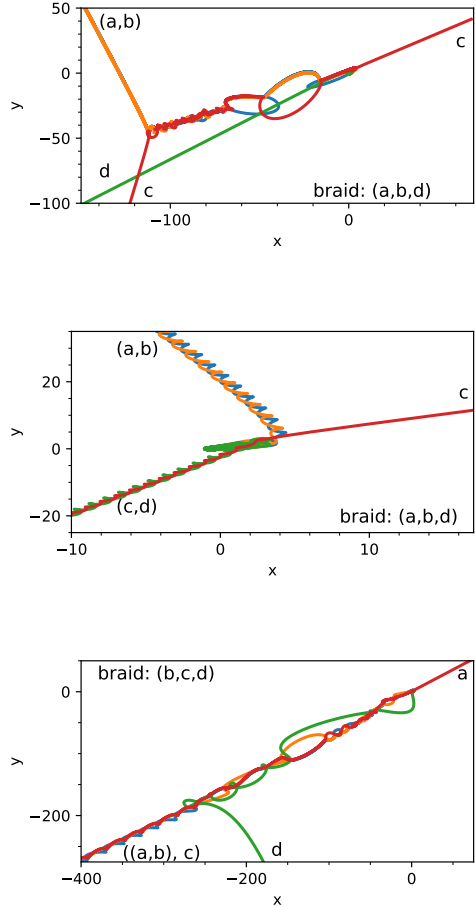


Fig. 4. Three examples of how the braid $I.A.4^{i.c.}(0.5)$ forms from an encounter between a binary (a,b) and two single stars (c) and (d), between two binaries (a,b), and (c,d), and a triple ((a,b),c) encountering a single (d).

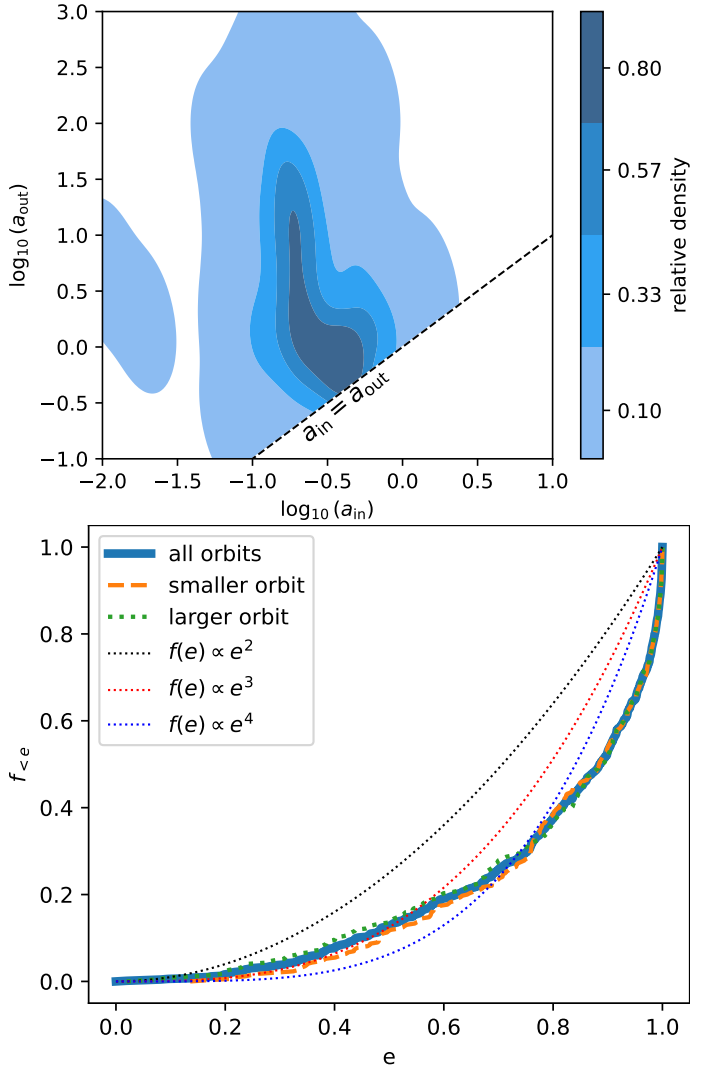


Fig. 5. Model A distributions of orbital elements, semi-major axis and eccentricity for interaction Model A, resulting in a binary-binary with $f_{BB} = 0.058$ (see table 2). The top panel shows the semi-major axis of the two binaries, where we present the tighter binary along the x-axis and the wider binary along the y-axis (explaining the empty lower right corner bordered by the dashed line). The bottom panel shows the eccentricity distributions of various orbits. The Kolmogorov-Smirnov test indicates that for model A, the tighter and wider distributions for eccentricity are indistinguishable. For the Figure-8 ($p = 0.0064$) and $I.A.4^{i.c.}(0.5)$ ($p = 0.034$) the eccentricity distribution of the tighter binaries appears not to be randomly sampled from a single parent distribution.

Model	$v_{in} = 0$			$v_{in} = 2$		
	D_{BSS}	D_{BB}	D_{TS}	D_{BSS}	D_{BB}	D_{TS}
Figure-8	1.0	0.4	0.2	1.0	0.4	0.4
Model A	0.9	0.2	0.2	0.8	0.6	0.1
$I.A.4^{i.c.}(0.5)$	1.2	0.1	0.3	1.1	0.5	0.4
$I.A.68^{i.c.}(0.5)$	0.9	0.2	0.2	0.8	0.3	0.3

Table 4. Fractal (box counting) dimension for the distributions over azimuth and polar angles for the various simulation outcomes for braids Figure-8, Model A, $I.A.4^{i.c.}(0.5)$, and $I.A.68^{i.c.}(0.5)$ (as in table 3). Here D_{BSS} , D_{BB} , and D_{TS} give the box counting dimension for the binary-single-single, binary-binary, and triple-single results. Note the value of D_{ts} for Model A is indicated as an order of magnitude estimate, because the number of successful simulations was too small to make a reliable estimate of the fractal dimension.

the amount of data in our experiment is rather limited, we argue that these clusterings are related to the chaotic behavior of four-body encounter. A similar clustering and patched stability was observed in three-body encounters as islands of stability in a sea of chaos Trani et al. (2024).

4.7. The effect of numerical accuracy

In our experiment, we rely on the reversibility of Newton's equations of motion. However, the numerical method adopted is not precisely time reversible. We did not perform converged solution simulations because our analysis is strictly of a statistical nature. Small errors when integrating in one direction, may indeed result in failing the reversible solution to lead to the same initial conditions. In principle, this would render the numerical result apprehensive Portegies Zwart & Boekholt (2018).

The interactions, however, are generally short (lasting < 10 braid orbits), and the original braids have a long Lyapunov time scale ($\gtrsim 1000$ orbits). As a consequence, the chaotic behavior of the systems hardly has time to cause numerical errors to grow substantially. The vast majority of interactions have a relative

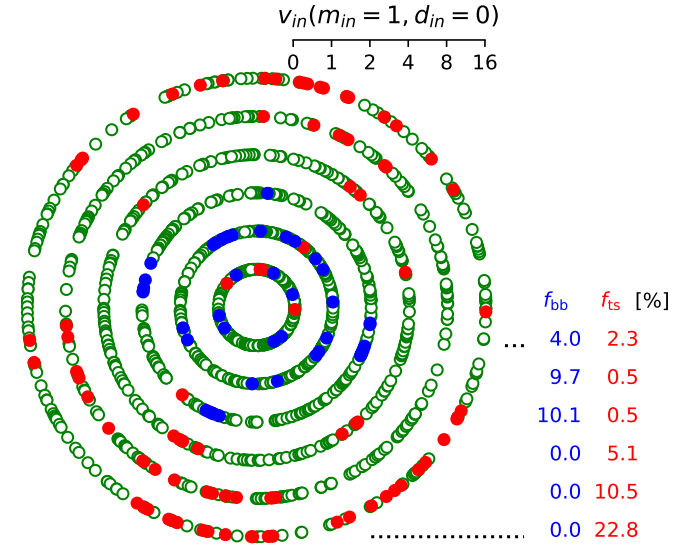
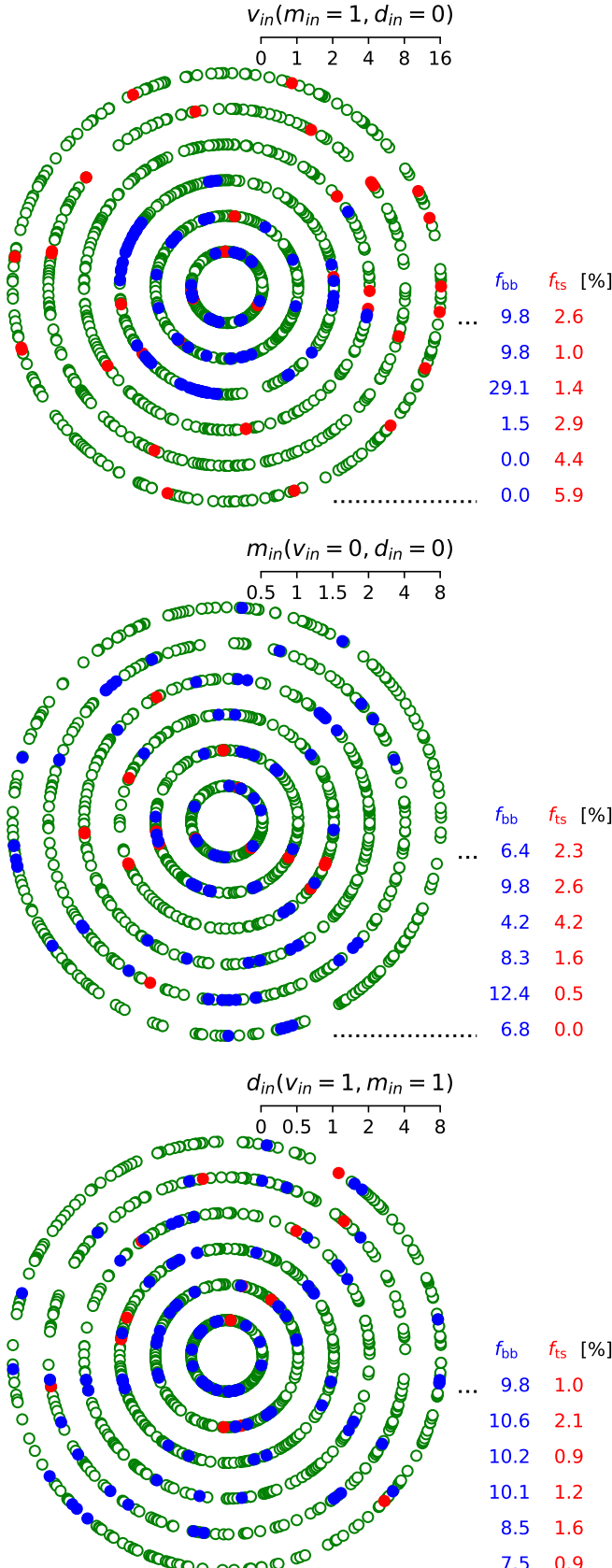


Fig. 7. same as figure 6 but for braid $I.A.68^{i.c.}(0.5)$.

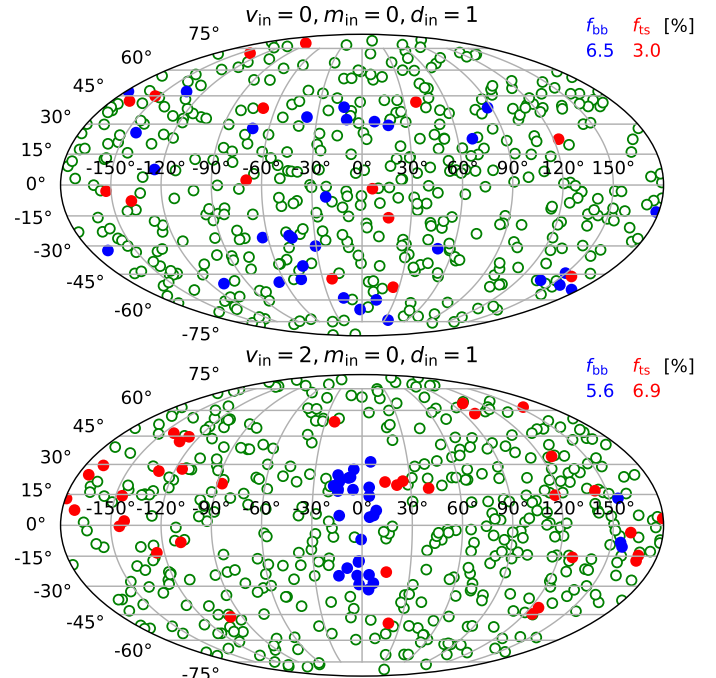


Fig. 8. Mollweide projection (azimuth along the x-axis and polar angle) for encounters of the figure 8 braid with $v_{in} = 0$ (top panel) and $v_{in} = 2$ (bottom panel). The other parameters are $m = 1$, $d = 0$. Each simulation is run 300 times with $\eta = 0.01$. For the legend of the symbols see also figure 6.

energy error $< 10^{-5}$, which should suffice for a statistical scientific interpretation. In some cases, the energy error at the end of the simulation is larger, but these are not systematically associated to one of the interactions of interest. We therefore consider our results robust, and not systematically affected by numerical effects.

To further support this, we perform an additional series of simulations based on the Figure-8 braid. In figure 9 we present the effect of numerical accuracy on the simulation results. Each circle shows the results (see the legend in and explanation in figure 6) for a series of simulations for a specific value of the time-step parameter η , which we varied from 0.01 (inner most

Fig. 6. Result of the encounter with Model A when varying v_{in} (top panel), m_4 (middle panel), and d_{in} (bottom) for 6 values of the free parameter. The results are presented along the circle ϕ , and the parameter value corresponding to the concentric circles are indicated along the scale bar on the top middle to right of each figure. To the bottom right, we show the fraction of interactions that resulted in a binary-binary (blue), and to a triple-single (red). These colors correspond to the colors of the bullets in the concentric circles: blue for binary-binary, red for triple-single, and open green circles for the most common result of a binary with two singles. For comparison, the circle in the top panel is identical to the second (from the inside) circle in the middle panel. The second circle in the top panel is identical to the inner circle in the bottom panel.

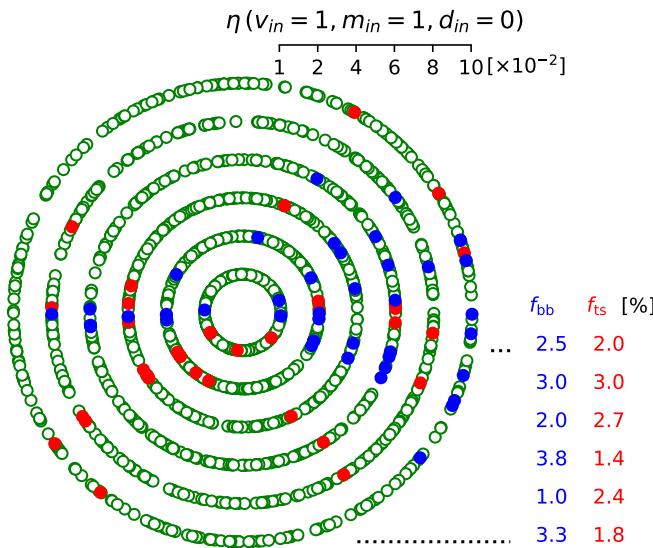


Fig. 9. Result of the encounter for the Figure-8 braid for $v_{in} = 1$, $m_{in} = 1$, $d_{in} = 0$, but for various values of the numerical time-step parameter η . The latter tunes the time-step of the numerical integration. The default choice in our simulations $\eta = 0.01$ (represented by the inner most circle), is here relaxed for circles further out. Circles further out represent less accurate integration. Each set of runs contains 300 solutions for that particular value of η .

circle) to 0.1 (outer most circle). Not shown is a series of runs for $\eta = 0.001$, but the results are statistically indistinguishable from $\eta = 0.01$.

The various fractions of simulation outcomes are presented to the right of the figure (as in figure 6). For this case, the canonical rate at which a braid forms from two binaries is about 2.6 with a comparable dispersion. Statistically, the probability of a braid forming through a binary-binary encounter or through a triple-single encounter are independent of integration accuracy.

5. Conclusion

We integrated four different three-body braids, perturbing them with a fourth particle and evolving until dissolution. Most braids separated into a binary plus two singles; $\sim 5\%$ yielded two binaries, and $\sim 3\%$ formed a triple with one escaper.

When the incoming velocity exceeds the braid's binding energy, the braid may survive temporarily. Symmetric braids dissolve readily under such strong perturbations, while less symmetric ones may survive if encountered along the short axis. For instance, braid $I.A.68^{i.c.}(0.5)$ withstands broadside impacts, whereas model A breaks into four singles or a binary with two singles.

Reversing ionizing encounters confirms Figure-8 braids can form from encounters between two binaries (Heggie 2000). These binaries typically have high eccentricities, $\langle e \rangle = 0.80 \pm 0.22$, with a distribution skewness ($S_k \sim -1.26$) to even higher eccentricities, exceeding typical Galactic ($\langle e \rangle \sim 0.6$) and Kuiper belt ($\langle e \rangle \sim 0.2$) binaries, implying favored initial binary parameters are uncommon.

Braid-formation cross sections for binary-binary ($\sim 5\%$) to triple-single ($\sim 3\%$) encounters, partially offsetting the rareness of suitable binaries. Near-coplanar orbital planes, however, are required, further restricting formation. Despite this, considering triples and diverse configurations, braids may be quite common in the Galaxy (Heggie 2000).

Although the majority of calculations was performed in a plane, we relax this assumption by allowing non-planar interactions. Although, our parameter-space coverage for this generalized approach is limited to varying a few of the free parameters over limited range, our findings show that braids can form a wide range of parameters, including non-planar encounters.

We observe that the parameter-space distribution of forming braids is anisotropic and has a relatively low fractal dimension, forming distributions in azimuth and polar angles in a 2-dimensional space much like the earlier work of Jackson Pollock rather than his late works, rather than his late works. The anisotropy of the initial parameter space becomes more pronounced for higher incoming velocities.

Braids are more likely to survive in shallow gravitational potentials, e.g., trans-Neptunian objects, Oort cloud, Galactic halo, or intergalactic space. The high Kuiper belt binary fraction supports transient braids in these regions (Noll et al. 2008).

Finite object sizes of astronomical objects suggest braids can form from collisions during binary-binary or binary-triple interactions. Stellar braids often lead to collisions unless objects are compact, suggesting black hole or neutron star braids might form and be detectable via gravitational waves. In addition, massive high velocity runaway stars could form from ionized braids, as one (or both) of the binaries in which the braid dissolves is prone to the two stars colliding.

Data availability

All data generated for this paper will be made available on Zenodo. The braid-generating and integrating scripts are available through the AMUSE package at amusecode.org.

Code availability

All work was done with AMUSE, and the cripts for reproducing this experiment are available via amusecode.org.

Acknowledgements

We thank Douglas Heggie, Anna Lisa Varri, and Tjarda Boekholt for discussing braids. We also thank the referee for the suggestion to include a discussion on the non-planarity of the problem. SPZ is deeply indebted to his friend Joost Visser for joining the expedition by ferry and train to Edinburgh and attending the Edinburgh Chaotic Rendez-vous in September 2025.

References

- Alvarez-Ramirez, J., Ibarra-Valdez, C., & Rodriguez, E. 2016, Chaos, Solitons & Fractals, 83, 97
- Boekholt, T. & Portegies Zwart, S. 2015, Computational Astrophysics and Cosmology, 2, 2
- Chenciner, A., Gerver, J., Montgomery, R., & Simó, C. 2002, Simple Choreographic Motions of N Bodies: A Preliminary Study, ed. P. Newton, P. Holmes, & A. Weinstein (New York, NY: Springer New York), 287–308
- Chenciner, A. & Montgomery, R. 2000, Annals of Mathematics, 152, 881
- Ginat, Y. B. & Perets, H. B. 2024, MNRAS, 531, 739
- Heggie, D. C. 1975, MNRAS, 173, 729
- Heggie, D. C. 2000, MNRAS, 318, L61
- Heggie, D. C. & Mathieu, R. D. 1986, in Lecture Notes in Physics, Berlin Springer Verlag, Vol. 267, The Use of Supercomputers in Stellar Dynamics, ed. P. Hut & S. L. W. McMillan, 233
- Henon, M. 1976, Celestial Mechanics, 13, 267
- Homburg, A. J. & Knobloch, J. 2024, Bifurcation Theory, Vol. 246 (American Mathematical Society)
- Kajihara, Y., Kin, E., & Shibayama, M. 2023, Topology and its Applications, 337, 108640

Kapela, T. & Simó, C. 2007, *Nonlinearity*, 20, 1241

Kepler, J. 1609, *Astronomia nova*, Vol. 1

Li, X., Jing, Y., & Liao, S. 2018, *Publ. Astr. Soc. Japan*, 70, 64

Li, X., Li, X., & Liao, S. 2021, *Science China Physics, Mechanics, and Astronomy*, 64, 219511

McMillan, S., Portegies Zwart, S., van Elteren, A., & Whitehead, A. 2012, in *Astronomical Society of the Pacific Conference Series*, Vol. 453, *Advances in Computational Astrophysics: Methods, Tools, and Outcome*, ed. R. Capuzzo-Dolcetta, M. Limongi, & A. Tornambè, 129

Montgomery, R. 1998, *Nonlinearity*, 11, 363

Moore, C. 1993, *Phys. Rev. Lett.*, 70, 3675

Newton, I. 1687, *Philosophiae Naturalis Principia Mathematica*, Vol. 1

Noll, K. S., Grundy, W. M., Chiang, E. I., Margot, J.-L., & Kern, S. D. 2008, *Binararies in the Kuiper Belt*, ed. M. A. Barucci, H. Boehnhardt, D. P. Cruikshank, A. Morbidelli, & R. Dotson, 345–363

Orwell, G. 1949, *Nineteen Eighty-Four* (London: Secker & Warburg), first edition published June 8, 1949

Poincaré, H. 1891, *Bulletin Astronomique*, Serie I, 8, 12

Portegies Zwart, S. & McMillan, S. 2018, *Astrophysical Recipes: The art of AMUSE*

Portegies Zwart, S., McMillan, S., Harfst, S., et al. 2009, *New Astronomy*, 14, 369

Portegies Zwart, S. F. & Boekholt, T. C. N. 2018, *Communications in Nonlinear Science and Numerical Simulations*, 61, 160

Portegies Zwart, S. F., Boekholt, T. C. N., Por, E. H., Hamers, A. S., & McMillan, S. L. W. 2022, *A&A*, 659, A86

Schubart, J. 1956, *Astronomische Nachrichten*, 283, 17

Simó, C. 2001, in *European Congress of Mathematics: Barcelona*, July 10–14, 2000, Volume I, Springer, 101–115

Simó, C. 2002, in *Contemporary Mathematics*, Vol. 292, 209–228

Simó, C. 1994, *Publication details or conference proceedings*

Terracini, S. 2022, *n-Body Problem and Choreographies*, ed. G. Gaeta (New York, NY: Springer US), 357–389

Trani, A. A., Leigh, N. W. C., Boekholt, T. C. N., & Portegies Zwart, S. 2024, *A&A*, 689, A24